

# Electrical Double Layer Properties of Spherical Oxide Nanoparticles

Christian Hunley and Marcelo Marucho<sup>1</sup>

*Department of Physics and Astronomy, The University of Texas at San Antonio, San Antonio, TX  
78249-5003*

---

## Abstract

The accurate characterization of electrical double layer properties of nanoparticles is of fundamental importance for optimizing their physicochemical properties for specific biotechnological and biomedical applications. In this article, we use classical solvation density functional theory and a surface complexation model to investigate the effects of pH and nanoparticle size on the structural and electrostatic properties of an electrolyte solution surrounding a spherical silica oxide nanoparticle. The formulation has been particularly useful for identifying dominant interactions governing the ionic driving force under a variety of pH levels and nanoparticle sizes. As a result of the energetic interplay displayed between electrostatic potential, ion-ion correlation and particle crowding effects on the nanoparticle surface titration, rich, non-trivial ion density profiles and mean electrostatic potential behavior have been found.

---

*Keywords:* Electrical double layer, Ion distribution, Density functional theory, Nanoparticles, Surface chemistry

## 1. Introduction

An increasing number of nanoparticle applications have been recently proposed in which the pH level of the liquid solution might have a high impact on their functional behavior<sup>1-4</sup>. Consequently, there is a high demand in taking control of the mechanisms

---

<sup>1</sup>Email:marcelo.marucho@utsa.edu

governing this process to optimize the physicochemical properties of nanoparticles for specific biotechnological and biomedical applications<sup>5-8</sup>. Having this ability requires an accurate molecular understanding of the structural and electrostatic properties of liquids surrounding nanoparticles. A large number of research papers published on colloidal systems reveal a complex, even not well understood, interplay between the surface charge density (SCD), Zeta potential (ZP), nanoparticle size (NS), ionic charge, water density distributions and pH levels of the surrounding aqueous solution. These articles provide insight on the formation of electric double layers (EDLs) where the electrostatic and entropic interactions between the nanoparticle and the aqueous medium generate a strongly correlated liquid near the surface of the nanoparticle<sup>9-14</sup>. One major source of complexity in describing EDL properties comes from the still not fully elucidated role of the pH level on the electrostatic ion-ion correlation<sup>15,16</sup>, entropy (e.g. particle crowding)<sup>17</sup> and mean electrostatic potential that contribute to the ionic driving force<sup>18</sup>. Gaining this understating at the microscopic level is indeed challenging, sometimes impossible, to obtain using current experimental techniques and conventional mean field-like Poisson Boltzmann (PB) approaches<sup>19-21</sup>. More sophisticated approaches were proposed to overcome a number of these limitations<sup>22-31</sup>. A novel approach named classical solvation density functional theory (CSDFT) has been recently introduced to study the influence that biological environments at neutral pH may have on the physicochemical properties of spherical nanoparticles of different sizes while under a variety of electrolyte conditions<sup>32</sup>. A more recent formulation of this approach combines CSDFT and surface complexation model (SCM)<sup>30</sup> to account for ion-ion correlation and particle crowding effects on the surface titration of spherical oxide nanoparticles<sup>31</sup>. The results, successfully validated against experiments, show that the particle crowding and electrostatic screening effects have a profound influence on the SCD and ZP of the nanoparticle.

In this article, we extend the aforementioned work by presenting a comprehensive analysis to advance the understanding of the role that pH and nanoparticle size play

on the structural and electrostatic properties of the electrolyte surrounding spherical oxide nanoparticles. We consider spherical  $SiO$  nanoparticles with sizes of different order of magnitude immersed in a monovalent electrolyte of acid and alkaline aqueous solutions. We use CSDFT and SCM to calculate the water and ion density profiles as well as the mean electrostatic potential (MEP) arising from the charging process generated by the nanoparticle surface chemistry. Additionally, we calculate the particle crowding, ion-ion correlation and electrostatic energy contributions to the ionic potential of mean force (PMF) to identify the dominant interactions governing the EDL properties. Finally, we compare our results against Poisson-Boltzmann (PB) predictions to determine the role that the corrections to the continuum model have in capturing charge inversion, ionic layering formation, and other important phenomena characterizing these colloidal systems.

## 2. Theory

In this section we provide the basic formulation of the approach used in this article. The detailed description can be found in references<sup>31,32</sup>.

### 2.1. Classical solvation density functional theory for spherical electrical double layers

In this approach, we consider a rigid charged spherical nanoparticle of radius  $R$  and uniform surface charge density  $\sigma$  surrounded by an electrolyte solution comprised of  $m$  ionic species. We use the solvent particle model to characterize the electrolyte<sup>31</sup>. Each ionic species  $i$  is represented by bulk Molar concentration  $[\rho_i^0]$ , a charged hard sphere of diameter  $d_i$ , and total charge  $q_i = ez_i$ , where  $e$  is the electron charge and  $z_i$  is the corresponding ionic valence (see Fig. 1(b)). Additionally, the solvent molecules are represented as a neutral ion species whereas the solvent electrostatics is considered implicitly by using the continuum dielectric environment with a dielectric constant  $\epsilon = 78.5$ . The nanoparticle-liquid interaction induces inhomogeneous ion profiles  $[\rho_i(r)]$  which are calculated using CSDFT as follows:

$$[\rho_i(r)] = \begin{cases} [\rho_i^0] \exp\{\Delta E_i(r, \{\rho_j\})\}, r > R + d_i/2 \\ 0, r \leq R + d_i/2 \end{cases} \quad (1)$$

where  $\Delta E_i(r, \{\rho_j\}) \equiv -\beta q_i \psi(r, \{\rho_j\}) + \Delta c_i^{(1)hs}(r; \{\rho_j\}) + \Delta c_i^{(1)res}(r; \{\rho_j\})$  stands for the ionic PMF per unit of thermal energy  $KT$ ,  $\beta = 1/kT$ ,  $k$  is the Boltzmann constant,  $T$  the temperature ( $=298.15\text{K}$ ), and  $c_i^{(1)hs}(r; \{\rho_j\})$  and  $c_i^{(1)res}(r; \{\rho_j\})$  are the hard sphere (particle crowding) and residual electrostatic ion-ion correlation functions, respectively.  $\psi(r, \{\rho_j\})$  represents the MEP for spherical nanoparticles

$$\psi(r, \{\rho_j\}) = \frac{e}{\epsilon} \int_r^\infty \frac{dr'}{r'^2} \left\{ \frac{4\pi R\sigma}{e} + 4\pi \int_0^{r'} dr'' r''^2 \sum_i z_i \rho_i(r'') \right\} \quad (2)$$

which is the formal solution of the PB equation for an homogeneous anisotropic dielectric media  $\epsilon$

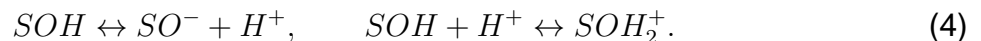
$$\nabla^2 \psi(r, \{\rho_j\}) = -\frac{1}{\epsilon} \sum_{i=1}^m z_i [\rho_i(r)] \quad (3)$$

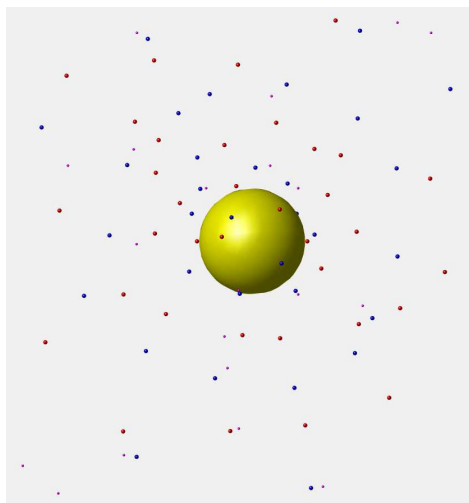
$$\epsilon \partial \psi(r, \{\rho_j\}) / \partial r |_{r=s} = -\sigma, \quad \psi(r, \{\rho_j\}) |_{r \rightarrow \infty} \rightarrow 0,$$

with the surface charge layer position defined as  $s \equiv R + \langle \{d_i\} \rangle$  and  $\langle \{d_i\} \rangle \equiv N_A l_B^3 \sum_i z_i^2 [\rho_i^0] d_i / (2m)$ . In the later definition  $N_A$  and  $l_B$  stand for the Avogadro number and the Bjerrum length, respectively.

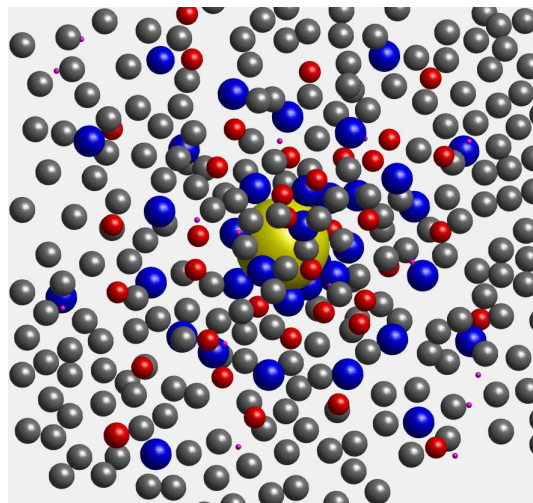
## 2.2. Surface complexation model

In order to account for the titration that regulates the nanoparticle surface charge density  $\sigma$  we consider the following two protonation reactions of single SO-coordinated sites :





(a) Poisson\_Boltzmann (PB) model



(b) Classical Solvation Density Functional (CSDFT) Model

Figure 1: In both models the Silica nanoparticle is displayed at the center of the figure in yellow color whereas  $Na^+$ ,  $Cl^-$  and  $H^+$  ions surrounding the nanoparticle are displayed in blue, red and magenta colors, respectively. Additionally, water molecules are displayed in gray color in the CSDFT model. In both models the Silica nanoparticle is represented as a hard sphere with uniform charge density on the surface whereas ions are represented by point-like charged particles in PB model and charged hard spheres with crystalline size in CSDFT model<sup>27</sup>. In both models the electrostatics of water is treated implicitly by using the continuum dielectric, but CSDFT additionally includes the water steric interaction explicitly by considering the water molecules as a neutral hard sphere (uncharged ions) at experimental size and concentration.

with equilibrium constants  $K_A$  and  $K_B$

$$K_A = \frac{N_{SO^-} [H^+]_s}{N_{SOH}}, \quad K_B = \frac{N_{SOH_2^+}}{N_{SOH} [H^+]_s}. \quad (5)$$

In the above expressions,  $N_{SOH}$ ,  $N_{SO^-}$ , and  $N_{SOH_2^+}$  are the surface site densities of  $SOH$ ,  $SO^-$  and  $SOH_2^+$ , respectively.  $[H^+]_s$  is the concentration of  $H^+$  ions at the SCD position  $s$ , namely

$$[H^+]_s \equiv [\rho_H(s)] = [\rho_H^0] \exp\{\Delta E_H(s, \{\rho_j\})\}, \quad (6)$$

where  $\Delta E_H(s, \{\rho_j\}) = -\beta\zeta + \Delta c_H^{(1)hs}(s; \{\rho_j\}) + \Delta c_H^{(1)res}(s; \{\rho_j\})$  is the hydrogen PMF per unit of thermal energy  $KT$ ,  $\zeta \equiv \psi(s, \{\rho_j\})$  is the ZP, and  $\Delta c_H^{(1)hs}$  and  $\Delta c_H^{(1)res}$  represent the hydrogen hard sphere (particle crowding) and ion-ion correlation contributions, respectively. The bulk concentration of  $H^+$  ions is represented by  $[\rho_H^0]$ , which is related to the  $pH$  value of the bulk liquid at infinity dilution by the expression  $pH = -\text{Log}([\rho_H^0])$ . The total number site density of functional groups on the SCD position is  $N_{total} = N_{SO^-} + N_{SOH} + N_{SOH_2^+}$  and the SCD is  $\sigma = -F(N_{SO^-} - N_{SOH_2^+})$ , where  $F$  represents the Faraday constant. Writing the densities sites in terms of the equilibrium constants (6), the SCD can be calculated as follows:

$$\sigma = -FN_{total} \frac{K_A - K_B [[\rho_H(r)]_{r=s}]^2}{K_A + [\rho_H(r)]_{r=s} + K_B [[\rho_H(r)]_{r=s}]^2} \quad (7)$$

Note that expression (7) describes the effects of the structural and electrostatic properties of the electrolyte on the SCD, whereas the boundary condition in expression (3) accounts for the SCD effects on the structural and electrostatic properties of the electrolyte. Therefore, eqns (1)-(7) must be solved self-consistently.

### 2.3. Electrolyte solutions and surface titration characterization

In this work, we utilize the same parameters used in our previous work<sup>31</sup>. We consider silica oxide nanoparticles with total density number of active functional group  $N_{total} = 2 * 10^{-6} mol/m^2$  and equilibrium constants  $pK_A = -\log(K_A) = 6.8$  (protonation) and  $pK_B = -\log(K_B) = 1.7$  (deprotonation). We consider a single salt comprised of mono-valent ions ( $NaCl$ ). The  $pH$  of the solution is adjusted by adding  $NaOH$  and  $HCl$  solutions to the electrolyte. The resulting electrolyte solutions contain five ion species ( $Na^+$ ,  $Cl^-$ ,  $H^+$ ,  $OH^-$ ,  $H_2O$ ). The free proton and hydroxyl ion bulk concentrations are given by the well-known expressions  $[\rho_H^0] = 10^{-pH}$ , and  $[\rho_{OH}^0] = 10^{-(14-pH)}$ , respectively, and the bulk concentrations of the electrolyte are chosen to satisfy the bulk electroneutrality condition.

### 2.4. PB approach

PB is a particular case of the CSDFT approach. Indeed, the expressions introduced in sections 2.1-2.3 for CSDFT recover the (non linear) PB approach by setting all ion sizes equal to zero (see Fig. 1(a)). In particular,  $s = R$ ,  $\Delta c_i^{(1)res}(r; \{[\rho_j]\}) = 0$ , and  $\Delta c_i^{(1)hs}(r; \{[\rho_j]\}) = 0$  in continuum models.

## 3. Results and discussion

In this section, we present and discuss the results predicted by CSDFT to elucidate the role that pH and nanoparticle size play on the EDL properties of silica oxide nanoparticles. Subsequently, we compare CSDFT and PB results to remark the physics going beyond continuum models. Note the Figures showing dashed and solid lines represent CSDFT and PB predictions, respectively.

### 3.1. CSDFT Results

In our first analysis we study a  $5\text{\AA}$  nanoparticle size in  $0.8M$  monovalent electrolyte solution. Overall, our results show a high impact of the pH level on the structural and electrostatic properties of spherical electrical double layers. This behavior comes from

expression (5) which explicitly establishes the influence of pH level and equilibrium constants on the number of active functional groups deprotonated ( $N_{SO^-}$ ) and protonated ( $N_{SOH_2^+}$ ) on the surface, namely

$$\begin{aligned} N_{SO^-} &= N_{SOH} 10^{-6.8+pH} \exp(-\Delta E_H) \\ N_{SOH_2^+} &= N_{SOH} 10^{-1.7-pH} \exp(\Delta E_H) \end{aligned} \quad (8)$$

where  $\exp(\Delta E_H)$  represents the normalized hydrogen density evaluated at the surface charge position  $s$ . This value can be estimated by the height of the first peak in the curves in Fig. 2 (a). Therefore, at low pH levels (e.g. 4 to 5), expression (8) predicts that the density number of active functional groups deprotonated are partially compensated by those protonated on the nanoparticle surface. This generates a poor charging mechanism which induces small surface charge densities (see eqn (7)) and generate weak nanoparticle-liquid electrostatic interactions. This phenomenon is shown in Fig. 3 on the counter-ionic and co-ionic PMF (dashed black and gray lines), where there is a lowering of the electrostatic potential energy (dashed light green and dark green lines) and the ion-ion correlation (dashed red and pink lines) contributions whereas the ionic entropy (dashed blue and cyan lines) contribution remains unchanged. According to this analysis, we arrived at the conclusion that the driving force governing the structural and electrostatic properties of the EDL in acid electrolyte solutions comes from the ionic entropy energy. This behavior of the ionic PMF generates ion density profiles characterized by an increase of the accumulation of co-ions ( $Cl^-$ ) and depletion of counter-ions ( $Na^+$ ) near the surface of the nanoparticle compared to those in bulk concentrations (Fig. 4 (a)-(b)). Interestingly, there is a higher accumulation of co-ions than counter-ions found in the first shell at low pH levels due to the ionic asymmetry size effects. Indeed, even though there is the same co-ions and counter-ions bulk concentration ( $=0.8M$ ), the size of the co-ions are larger than the counter-ions which induces larger entropic contributions to the ionic PMF (see dashed blue and cyan lines in Fig. 3). For instance, we find around 44 % more



$Cl^-$  than  $Na^+$  ions in the first shell at pH level 4. On the other hand, our results on MEP at low pH levels reveal charge inversion around a separation distance of 1.2 Å from the nanoparticle surface (Fig. 5 (a)). This is caused by an excess in counter-ion contributions to the MEP which generates a charge screening that overcompensates the electrostatic potential produced by the small nanoparticle charge. Additionally, the MEP near the nanoparticle surface is characterized by a non-monotonic short-range behavior. This non-trivial and counter-intuitive behavior of the MEP comes from expression (2) which explicitly establishes the role that pH plays on the surface charge density (first term) and ion density profiles (second term). At low pH levels, the first term becomes small whereas the second term provides the nontrivial behavior of the MEP near the nanoparticle surface. Moreover, the height of the first peaks in the counter-ion and co-ion density profiles are of the same order but the former are located closer to the nanoparticle surface dominating the contributions when integrated along the radial separation distances.

A different scenario is predicted by eqn (8) at higher pH levels (e.g. 6 to 8) where a large number of active functional groups are deprotonated and very few are protonated, thereby inducing large negative charge density on the nanoparticle surface. This behavior generates strong nanoparticle-liquid electrostatic interactions and, consequently, electrostatic energy contributions to the ionic PMF comparable in magnitude with the corresponding ionic entropy energy. In this case, unlike the results presented for low pH levels, the ionic driving force near the nanoparticle surface strongly depends on the ion species. For counter-ions specifically, we find that the electrostatic potential energy competes with the ionic entropy (particle crowding) energy by contributing both with positive values of the same order to the corresponding ionic PMF. On the other hand, our results for co-ions show that the electrostatic energy (negative values) is partially compensated by the ionic entropy contribution (positive values). This competition and balance behavior are depicted in Fig. 3 where we represent the ionic entropy contribution by dashed blue and cyan lines, the electrostatic potential energy contribution by dashed light green and

dark green lines, the ion-ion correlation contribution by dashed red and magenta lines, and the ionic potential of mean force by dashed black (counter-ionic) and gray (co-ionic) lines. As a result of this interplay, the structural properties of spherical EDLs in alkaline electrolyte solutions present a significant increase in the accumulation of counter-ions ( $Na^+$ ) and depletion of co-ions ( $Cl^-$ ) near the surface of the nanoparticle with respect to those in the bulk phase. Our results also reveal a more pronounced layering formation in counter-ions than co-ions. For instance, Figs. 4 (a)-(b) shows 5 times and 13 times higher accumulation of  $Na^+$  in the first shell than in the bulk solution at pH level 6 and 8, respectively. Whereas our results for  $Cl^-$  show 3.75 times and 1.5 times higher accumulation at pH level 6 and 8, respectively. In addition, our results reveal higher negative values and longer ranged asymptotic decay of the MEP at high pH levels (see dashed red and black lines in Fig. 5 (a)).

Certainly, the short-ranged nanoparticle-liquid entropic interactions are weakened at intermediate separation distances, e.g between  $\sim 12\text{\AA}$  and  $18\text{\AA}$  from the nanoparticle surface. Consequently, the MEP dominates the asymptotic behavior of the ionic PMF (see Fig. 3) as well as the pH effects on the structural and electrostatic properties of electrolyte solutions. Accordingly, an increase of pH levels induces large values of the PMF and generates slower asymptotic decay (see Fig. 5 (a)). This in turn generates a quasi-monotonic decay behavior in the ion density profiles (see Fig. 1 (a)-(b)). As expected, all nanoparticle-liquid interactions and pH effects on the electrolyte solution properties at longer separation distances vanish recovering the well-known electrolyte bulk properties. Overall, the EDL properties remain unchanged at pH level 10 and higher (results not presented in this article) because the nanoparticle reaches the charge saturation limit<sup>9,32</sup>.

In our second analysis we repeat the previous calculations for a larger nanoparticle size ( $= 580\text{\AA}$ ) in order to provide insight into the nanoparticle size effects on the structural EDL properties of silica oxide nanoparticles. Our results in Fig. 2 (a) and (b) show that the increase of the nanoparticle surface induces larger number of deprotonated functional

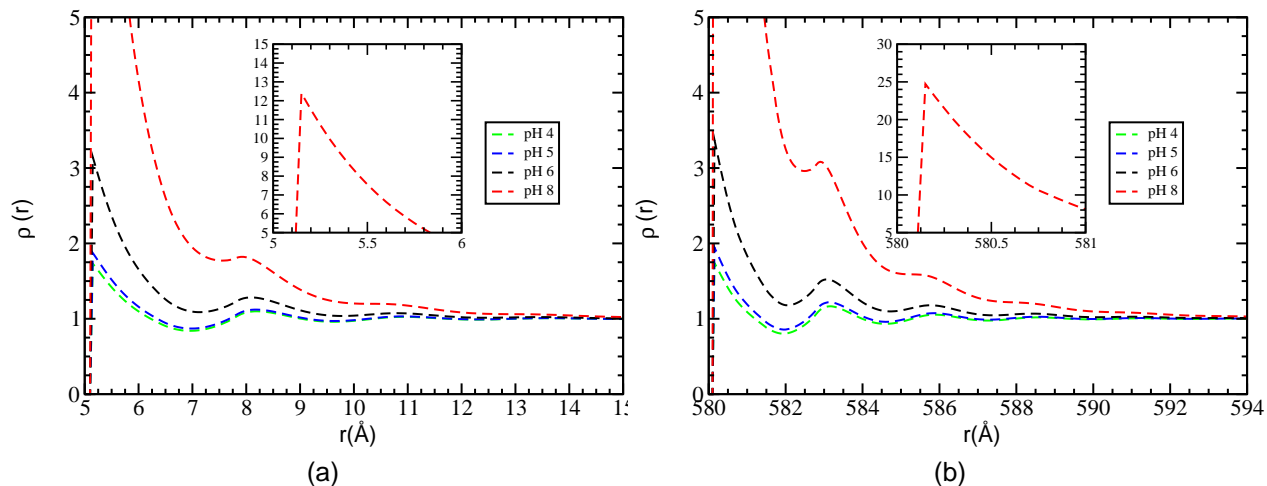


Figure 2: Hydrogen density profiles per bulk concentration predicted by CSDFT for  $0.8M$   $NaCl$  salt concentration. Green, blue, black and red represents the Hydrogen density profiles for pHs 4, 5, 6, and 8, respectively. Plot (a) corresponds to  $5\text{\AA}$  nanoparticle size whereas plot (b) corresponds to  $580\text{\AA}$  nanoparticle size.

groups and, consequently, an increase of the total nanoparticle charge. As a result, the corresponding values of the MEP are magnified while keeping the trends predicted for the smaller nanoparticle size (see Fig. 5 (a)-(b)). Additionally, the increase of nanoparticle size causes higher entropic interaction between the nanoparticle and the surrounding medium which in turn increases the particle crowding effects on the ionic density profiles (e.g. taller peaks) near the nanoparticle surface. As a result, we find a more pronounced layering formation for the larger nanoparticle size. For instance, we find around 25 % more water molecules (see Fig. 6), 122 % more  $Na^+$  ions and 33 % less  $Cl^-$  ions (see Fig. 4 (c)-(d)) accumulated in the first shell for  $580\text{\AA}$  than for  $5\text{\AA}$  nanoparticle size at pH level 8. Overall, our results on the ion density profiles and MEP show that the trends obtained on the EDL properties for a  $5\text{\AA}$  nanoparticle are magnified when the particle size is increased.

### 3.2. PB - CSDFT comparison

In our final analysis we calculate PB predictions on ion density profiles and MEP for  $5\text{\AA}$  nanoparticle size with the same electrolyte conditions analyzed in the previous sec-

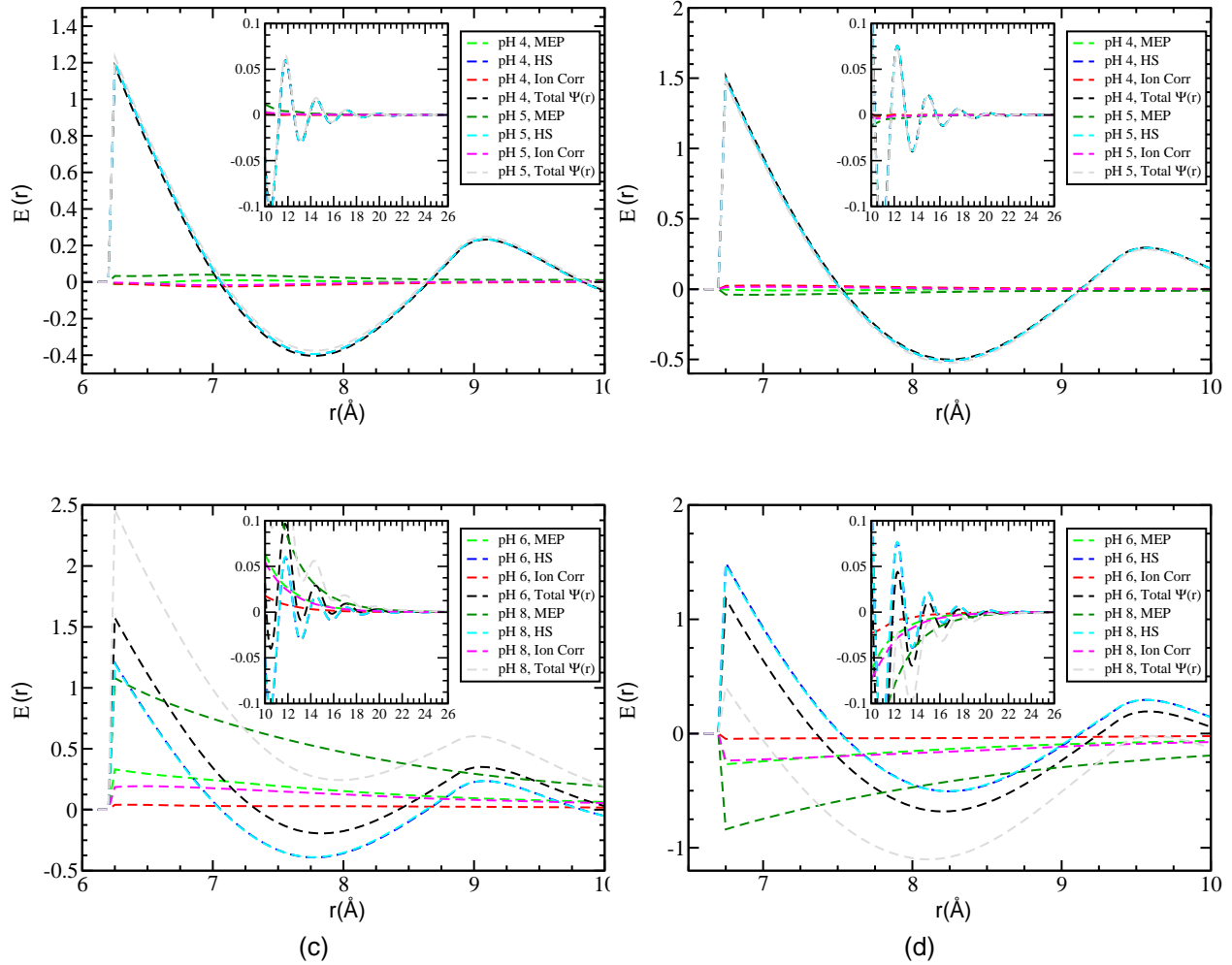


Figure 3:  $E(r)$  represents the mean electrostatic potential (=MEP), entropy (=HS), ion-ion correlation (=Ion Correl) and ionic potential of mean force (=Total  $\Psi$ ) energies per unit of thermal energy  $KT$  predicted by CSDFT for a  $0.8M$   $NaCl$  salt concentration and  $5\text{\AA}$  nanoparticle size. Light green and dark green colors correspond to MEP, blue and cyan colors correspond to entropy, red and magenta colors correspond to ion-ion correlation, and black and gray colors correspond to the ionic potential of mean force. Plots (a) and (b) represent the effects of low pHs (4 and 5) on  $Na^+$  and  $Cl^-$  ions, respectively, whereas plots (c) and (d) are those corresponding to the effects of high pHs (6 and 8).

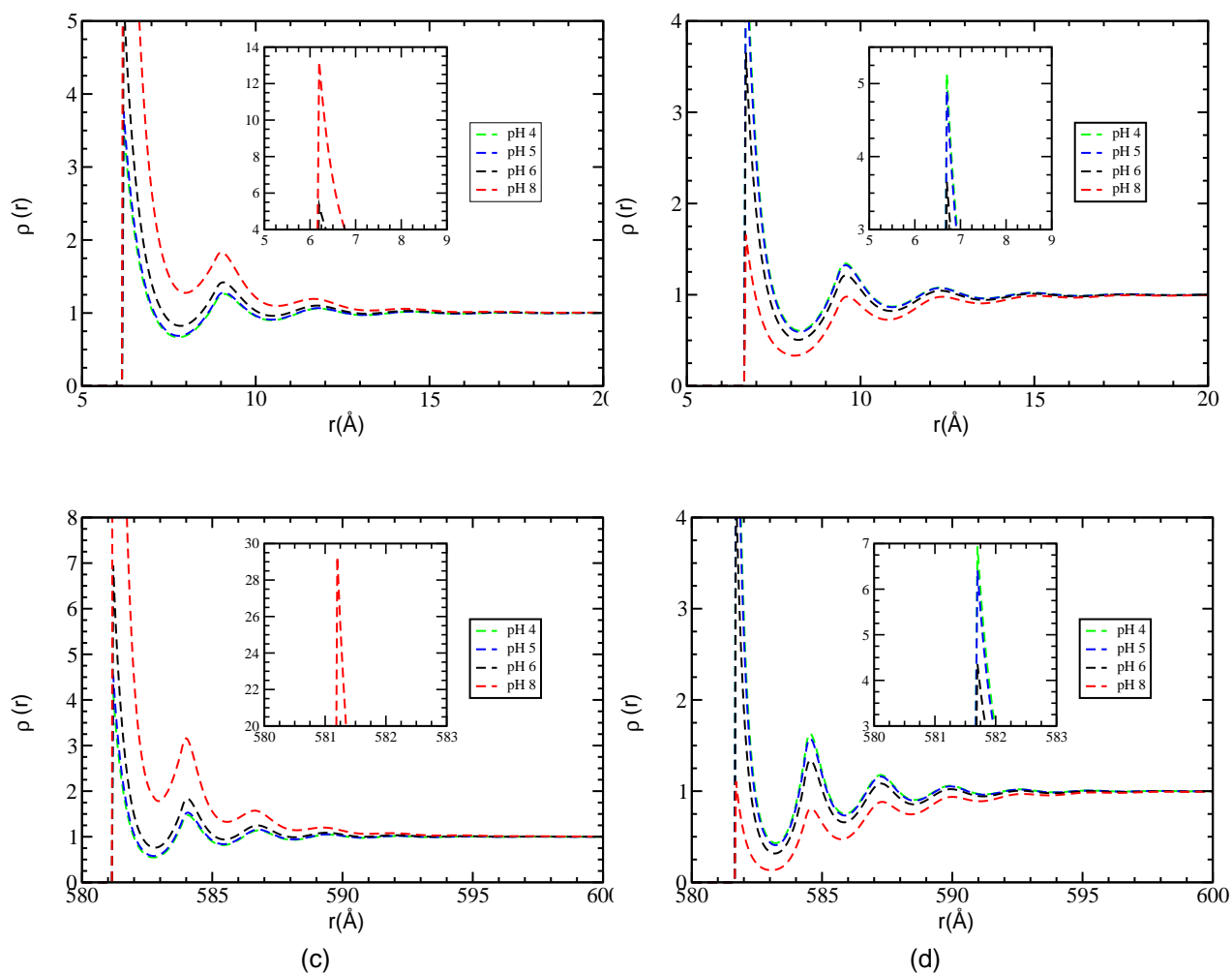


Figure 4: Ion density profiles per bulk concentration predicted by CSDFT for 0.8M  $NaCl$  salt concentration, 5Å and 580Å nanoparticle sizes, and several pH levels. Green, blue, black and red colors represent ion density profiles for pHs 4, 5, 6, and 8, respectively. Plot (a) and (c) show  $Na^+$  density profiles whereas plots (b) and (d) show  $Cl^-$  density profiles. Plots (a)-(b) and (c)-(d) correspond to 5Å and 580Å nanoparticle sizes, respectively.

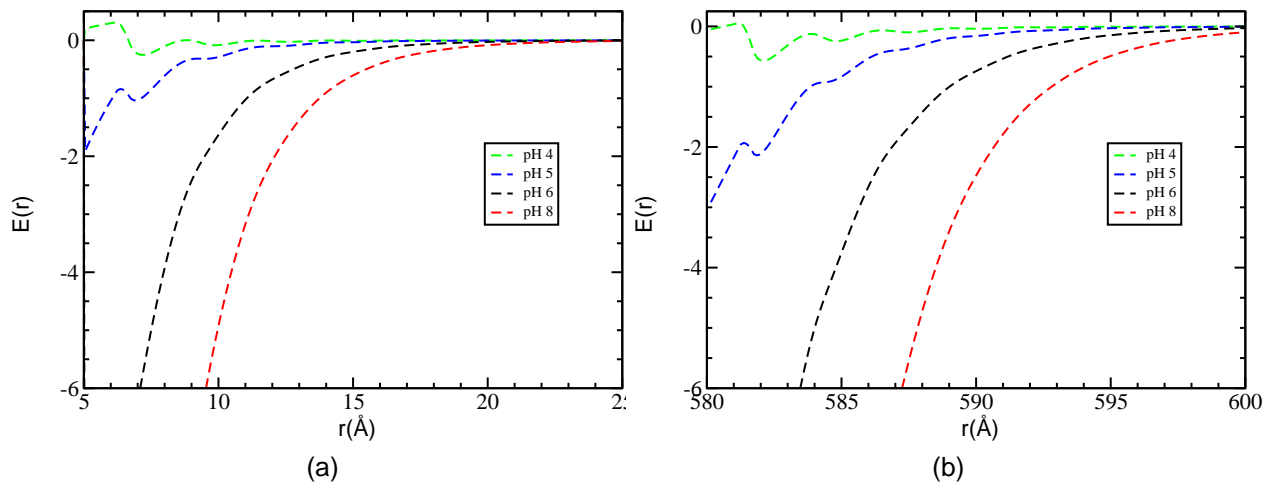


Figure 5: Mean electrostatic potential (MEP) per unit of thermal energy  $KT$  predicted by CSDFT for  $0.8M$   $NaCl$  salt concentration. Green, blue, black and red represents the MEP for pHs 4, 5, 6, and 8, respectively. Plot (a) corresponds to  $5\text{\AA}$  nanoparticle size whereas plot (b) corresponds to  $580\text{\AA}$  nanoparticle size.

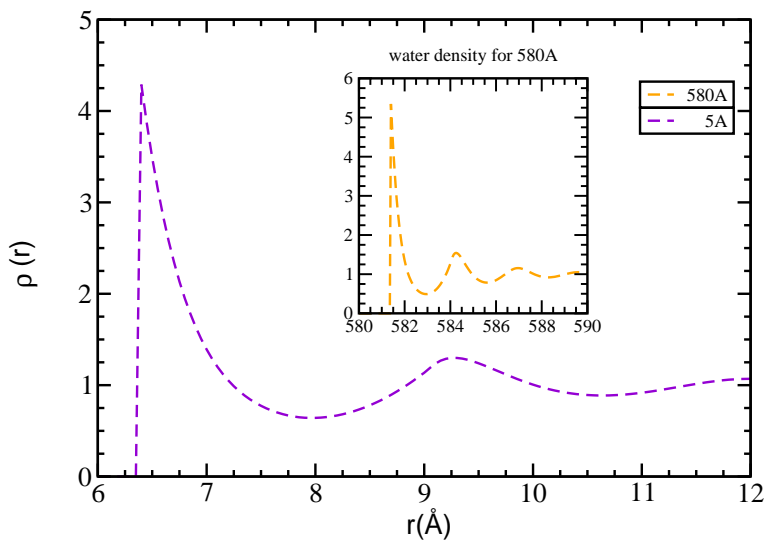


Figure 6: Water density profiles per bulk concentration predicted by CSDFT for  $0.8M$   $NaCl$  salt concentration and pH 4. Purple and orange dashed lines correspond to  $5\text{\AA}$  (and  $580\text{\AA}$ ) nanoparticle sizes, respectively.

tion. When comparing PB (solid lines in Fig. 7) with CSDFT results (dashed lines in Fig. 4-5), we observed consistency in trends for the MEP and ionic density profiles where long range contributions dominate, with significant deviations near the nanoparticle surface, in which the short range effects of the entropy and ion-ion correlation provide un-neglectable corrections to the PB predictions. These deviations are found to be more pronounced at low pH levels where the balance between the number of deprotonated and protonated functional groups on the nanoparticle surface significantly attenuate the solute-liquid electrostatic interaction. Among the differences between both approaches, it is worth mentioning that the PB approach is not able to capture layering formation, charge inversion or co-ion accumulation near the nanoparticle surface for any of the pH levels and nanoparticle sizes considered in this work. Clearly, the source of the differences is manifold. Firstly, the expression for the surface charge layer position used in CSDFT  $s \equiv R + N_A \lambda_B^3 \sum_i z_i^2 [\rho_i^0] d_i / (2m)$  generalizes the definition of continuum models ( $s = R$ ) by accounting for the ion diameters and bulk densities. As a result, it predicts SCD layering formation closer to the nanoparticle surface at low ionic densities for all ion sizes. On the other hand, it predicts longer deviation from the nanoparticle surface at 0.8M electrolyte concentration. This shift in the position of the SCD affects the evaluation of the ZP ( $\zeta \equiv \psi(r, \{\rho_j\})|_{r=s}$ ) generating lower CSDFT values compared to those predicted by PB []. Secondly, the ZP predicted by CSDFT also accounts for the ion-ion correlations, size asymmetry and particle crowding effects (see eqn. (1)), which are omitted in continuum models. Additionally, these two factors have a non-linear high impact effect on the titration and nanoparticle SCD properties (see eqn (7)). Another source of difference corresponds to the expression used by CSDFT to estimate the ionic PMF (see eqn (1)). Indeed, by considering not only electrostatic but also entropy and ion-ion correlation interactions, and in particular, by accounting for explicit water molecules at experimental size and concentration, CSDFT has been capable of capturing ionic layering formation and charge inversion, among other important features of colloidal systems. On

the contrary, these corrections to continuum models are attenuated at lower electrolyte concentrations, obtaining PB and CSDFT predictions in much better agreement<sup>1,9,32</sup>.

#### 4. Conclusion

In this article, we use classical solvation density functional theory (CSDFT) and a surface complexation model to investigate the effects of pH and nanoparticle size on the structural and electrostatic properties of an electrolyte solution surrounding a spherical silica oxide nanoparticle. This approach has shown to be an efficient and accurate computational tool in accounting for mean electrostatic potential (MEP), ion-ion correlation and ionic entropy (particle crowding) effects on surface titration. Additionally, the formulation has been able to capture the balance and competition between electrostatic and entropic contributions to the total ionic potential of the mean force (PMF). This feature has been particularly useful for identifying dominant interactions governing nanoparticle electrical double layer properties under a variety of pH levels and nanoparticle sizes. Overall, we find a high impact of the pH level on the structural and electrostatic properties of spherical electrical double layers in 5Å and 580Å nanoparticle sizes immersed in 0.8M monovalent electrolyte solution. At low pH levels, our results show small number of charged functional groups on the nanoparticle surface, and weak electrostatic interactions between the nanoparticle and surrounding liquid. Therefore, the resulting driving force governing the structural and electrostatic properties of the (EDL) in acid electrolyte solutions is found to come from the ionic entropy energy. The ion density profiles are characterized by an increase in accumulation of co-ions ( $Cl^-$ ) and depletion of counterions ( $Na^+$ ) near the surface of the nanoparticle, where asymmetry size effects are responsible for more co-ions inhabiting the first shell than counter-ions. Furthermore, our results on MEP reveal charge inversions and a non-trivial, non-monotonic short-range behavior. We find a different scenario at high pH levels where many functional groups are deprotonated on the nanoparticle surface. In this case, the ionic driving force near the nanoparticle surface is



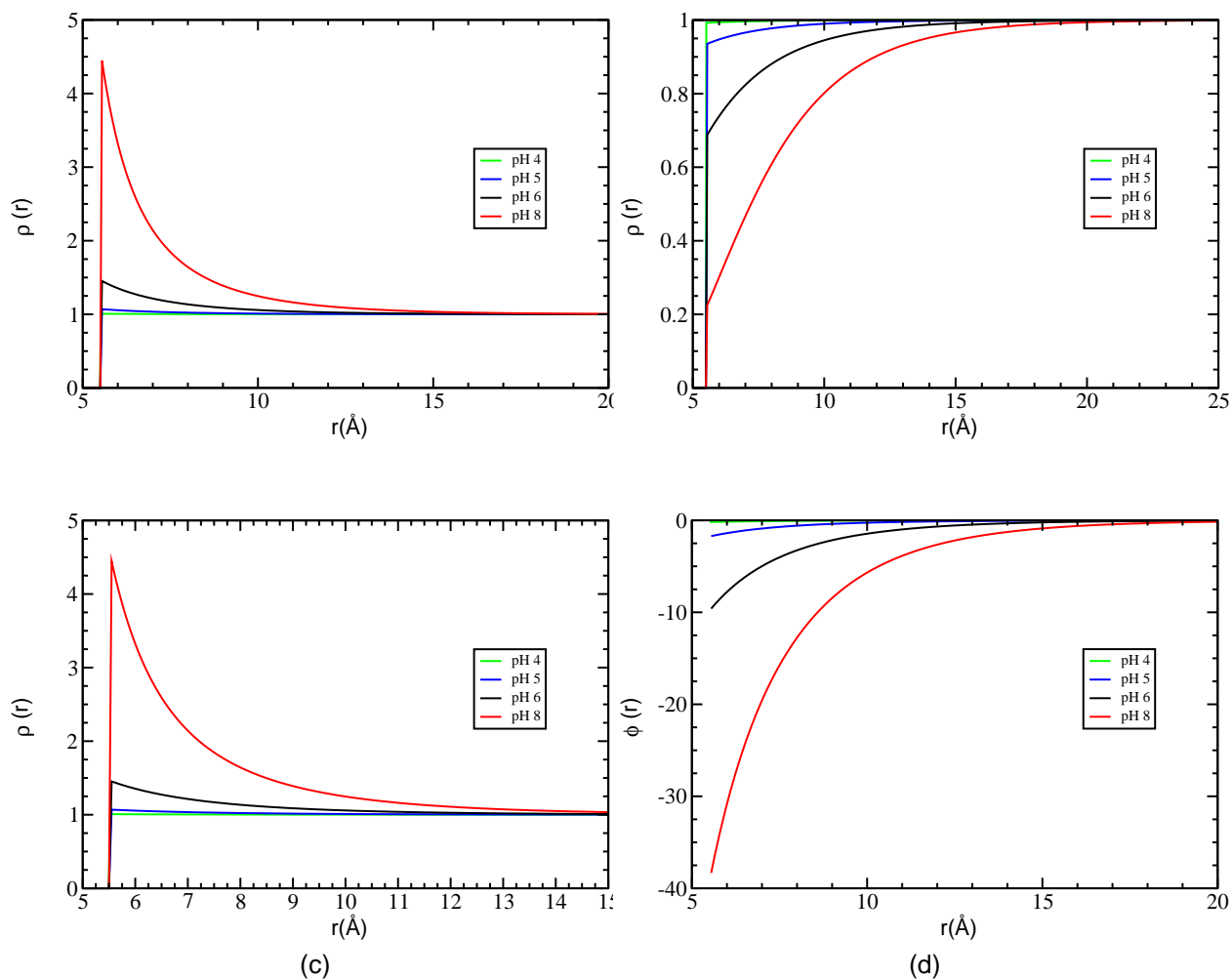


Figure 7: IPB results on  $0.8M NaCl$  salt concentration and  $5\text{\AA}$  nanoparticle size. Plots a, b and c correspond to  $Na^+$ ,  $Cl^-$ , and  $H^+$  density profiles normalized by bulk concentration, respectively. Plot d corresponds to the mean electrostatic potential (MEP) per unit of thermal energy  $KT$ . Green, blue, black and red solid lines represent the density profiles and MEP for pHs 4, 5, 6, and 8, respectively.

found to depend heavily on the ion species. For counter-ions, the electrostatic potential energy competes with the entropy, both providing with positive values of the same order to the ionic PMF. However, the electrostatic energy for co-ions is negative while entropy contributions remain positive, displaying a balancing relationship between them. As a result of this interplay, a reduced PMF governs the co-ion density distribution. We find a significant increase in the accumulation of counterions ( $Na^+$ ) and depletion of co-ions ( $Cl^-$ ) near the surface of the nanoparticle in alkaline electrolyte solutions. When comparing Poisson-Boltzmann (PB) with CSDFT results, we observed consistency in trends for the MEP and ionic density profiles where long range contributions dominate, with significant deviations near the nanoparticle surface, in which the short range effects of the hard sphere and ion-ion correlation provide unneglectable corrections to the PB predictions. These deviations are found to be more pronounced at low pH levels where the poor charging mechanism on the nanoparticle surface significantly attenuate the solute-liquid electrostatic interaction. Finally, our results on nanoparticle size effects show that increasing the nanoparticle surface and keeping fixed the other parameters of the model generates an increase of the nanoparticle charge and entropy interaction with the electrolyte solution. Consequently, the trends obtained on the EDL properties for a 5Å nanoparticle are magnified when the particle size is increased. Further research is currently in progress to study pH effects on cylindrical EDL properties. Future work involves the extension of the polar solvation classical density function theory, recently introduced by Drs. Varsasky and Marucho for planar geometries, to study polarization and pH effects on cylindrical and spherical EDLs.

## **Acknowledgments**

This work was partially supported by NIH Grant 1SC2GM112578-01.

## References

## References

- [1] S. Atalay, Y. Ma and S. Qian, *J. Colloid Interface Sci.*, 2014, 425, 128.
- [2] .Z. Abbas, C Labbez, S Nordholm and E Ahlberg, *J. Phys. Chem. C*, 2008, 112, 5715.
- [3] C. Pfeiffer, C. Rehbock, D. Huhn, C. Carrillo-Carrion, D. J. de Aberasturi, V. Merk, S. Barcikowski and W. J. Parak, *J. R. Soc. Interface*, 2013, 11 0931.
- [4] A. M. El Badawy, T. P. Luxton, R. G. Silva, K. G. Scheckel, M. T. Suidan and T. M. Tolaymat, *Environ. Sci. Technol*, 2010, 44, 1260.
- [5] G. Su, H. Zhou, Q. Mu, Y. Zhang, L. Li, P. Jiao, G. Jiang and B. Yan, *J. Phys. Chem. C*, 2012, 112 4993.
- [6] J.S. Souris, N. Chen, S. Cheng, C. Chen and L. Lo, *Cancer Theranostics*, ed. X. Chen and S. Wong, Academic Press, Oxford, 2014, 20, 363-391.
- [7] T.K Barik, B. Sahu and V. Swain, *Parasitol. Res.* 2008, 103, 253.
- [8] S. Honary and F. Zahir, *Trop. J. Pharm. Res.* 2013, 12, review 1, 255, review 2, 265.
- [9] M. Barisik, S. Atalay, A. Beskok and S.J. Qian, *J. Phys. Chem. C* 2014, 118, 1836.
- [10] Sonnefeld, M. Löbbus and W. Vogelsberger, *Colloids Surf. A*, 2001, 195 215.
- [11] J.H. Masliyah and S. Bhattacharjee, *Electrokinetic and Colloid Transport Phenomena*, John Wiley and Sons, Hoboken, 2006.
- [12] A. Studart, E. Amstad and L. Gauckler, *Langmuir* 2007, 23, 1081.
- [13] C. Merlet, D. Limmer, M. Salanne, R. Roij, P. Madden, D. Chandler and B. Rotenberg, *J. Phys. Chem. C*, 2014, 118, 18291.

- [14] L. B. Bhuiyan and C. W. Outhwaite, *Phys. Chem. Chem. Phys.*, 2004, 6, 3467.
- [15] C. Labbez, B. Jönsson, M. Skarba and M. Borkovec, *Langmuir*, 2009, 25, 7209.
- [16] G. I. Guerrero-Garcia, E. Gonzalez-Tovar, M. Quesada-Perez and A. Martin-Molina, *Phys. Chem. Chem. Phys.*, 2016, 18, 21852.
- [17] J. Israelachvili and H. Wennerström, *Nature*, 1996, 379, 219.
- [18] Z. Ovanesyan, B. Medasani, M. O. Fenley, G. I. Guerrero-Garcia, M. O. de la Cruz and M. Marucho, *J. Chem. Phys.*, 2014, 141, 225103 .
- [19] N. A. Baker, D. Bashford and D. A. Case, *New Algorithms for Macromolecular Simulation*, 2006, 49, 263.
- [20] Ren, P., Chun, J., Thomas, D.G., Schnieders, M.J., Marucho, M., Zhang, J. and Baker, N.A., *Quarterly Reviews of Biophysics*, 2012), 49, 427.
- [21] D. Andelman, *Soft Condensed Matter Physics in Molecular and Cell Biology*, W . C . K . Poon and D . Andelman, Taylor & Francis, New York, 2006, 6, 97–122.
- [22] P. Gonzalez-Mozuelos, G.I. Guerrero Garcia and M. O. de la Cruz, *J. Chem. Phys.*, 2013, 139, 064709.
- [23] A. Moncho-Jorda, J. A. Anta and J. Callejas-Fernandez, *J. Chem. Phys.*, 2013, 138, 134902.
- [24] G. I. Guerrero-Garcia, Y. Jing and M. O. de la Cruz, *Soft matter*, 2013, 9 6046.
- [25] C. N. Patra, *J. Phys. Chem. B*, 2010, 114, 10550.
- [26] C. N. Patra, R. Chnag and A. Yethiraj, *J. Phys. Chem. B*, 2004, 108, 9126.
- [27] C. N. Patra and A. Yethiraj, *J. Phys. Chem. B*, 1999, 103, 6080.
- [28] M. C Barbosa, M. Deserno and C. Holm, *Europhys. Lett.*, 2000, 52, 80.

- [29] K. Wang, Y. X. Yu and G. H. Gao, *Phys. Rev. E*, 2004, 70, 011912.
- [30] Z. Wang, L. Liu and I. Neretnieks, *J. Phys. Condens. Matter*, 2011, 23, 175002.
- [31] Z. Li and J. Wu, *Phys. Rev. E*, 2004, 70, 031109.
- [32] B. Medasani, Z. Ovanesyan, D.G. Thomas, M.L. Sushko and M. Marucho, *J. Chem. Phys.*, 2014, 140, 204510.
- [30] S. Goldberg, *Chemical equilibrium and reaction models*, in: R.H. Loeppert et al. (Eds.), *Soil Science Society of America Spec. Publ.*, Madison, WI, USA, 42, Soil Science Society of America, Madison, 1995.
- [31] Z. Ovanesyan, A. Aljzmi, M. Almusaynid, A. Khan, E. Valderrama, K. Nash and M. Marucho, *Journal of Colloid and Interface Science*, 2016, 462, 325-333.